https://doi.org/10.5194/egusphere-2023-629
Preprint. Discussion started: 13 April 2023

Determining the surface mixing layer height of the Arctic atmospheric boundary layer during polar night in cloudless and cloudy conditions

Elisa F. Akansu[1], Sandro Dahlke[2], Holger Siebert[1], and Manfred Wendisch[3]

[1]Leibniz Institute for Tropospheric Research (TROPOS), Leipzig, Germany
[2]Alfred Wegener Institute (AWI), Helmholtz Centre for Polar and Marine Research, Potsdam, Germany
[3]Leipzig Institute for Meteorology (LIM), Leipzig University, Germany

Correspondence: Elisa F. Akansu (akansu@tropos.de)

Abstract. This study analyzes turbulent properties in, and the thermodynamic structure of the Arctic atmospheric boundary layer (ABL) during winter and the transition to spring. These processes influence the evolution and longevity of clouds, and impact the surface radiative energy budget in the Arctic. For the measurements we have used an instrumental payload carried by a helium filled tethered balloon. This system was deployed between December 2019 and May 2020 during the yearlong Multidisciplinary drifting Observatory for the Study of Arctic Climate (MOSAiC) expedition. Vertically highly resolved in situ measurements of profiles of turbulent parameters were obtained reaching from the sea ice up to several hundred meters height. The two typical states of the Arctic ABL were identified: cloudless situations with a shallow and stable ABL, and cloudy conditions maintaining a mixed ABL. We have used profile data to estimate the height of the surface mixing layer. For this purpose, a bulk Richardson number criterion approach was introduced. By deriving a critical bulk Richardson number for wintertime in high latitudes, we have extended the analysis to radiosonde data. Furthermore, we have tested the applicability of the Monin-Obukhov similarity theory to derive surface mixing layer heights based on measured surface fluxes.

1 Introduction

The Arctic climate is changing rapidly and the complex Arctic climate system is sensitive to multiple intertwined mechanisms leading to an increased near surface air temperature, sea ice retreat, and further significant changes of Arctic climate parameters (Serreze and Barry, 2011). Atmospheric and cloud processes play an important role in understanding the currently ongoing climate changes in the Arctic (Wendisch et al., 2019). The enhanced response of the Arctic climate system to global warming is referred to as Arctic amplification. It includes feedback mechanisms, impacting factors, and sensitivity of the Arctic climate system. There are still significant gaps in understanding this phenomenon and uncertainties in modelling the driving processes (Wendisch et al., 2023). In particular, the processes determining the evolution of the Arctic atmospheric boundary layer (ABL) in cloudless and cloudy situations are not well characterized and represented by models (Wendisch et al., 2019). The ABL is the atmospheric layer above the Earth's surface whose effects are perceptible on small time scales (up to several hours) and refers to the region of the atmosphere that is directly influenced by the surface (Stull, 1988; Garratt, 1997). Especially during

https://doi.org/10.5194/egusphere-2023-629
Preprint. Discussion started: 13 April 2023

polar night, the vertical extend of the ABL plays an important role as stable stratification hampers the vertical exchange and leads to a near surface warming contributing to Arctic amplification mostly in the winter (Graversen et al., 2008; Bintanja et al., 2011). Models often fail in reproducing shallow ABLs in the Arctic (Esau and Zilitinkevich, 2010; Lüpkes et al., 2010).

To advance our knowledge on turbulent processes within the ABL, tethered balloon borne observations were performed during the yearlong Multidisciplinary Drifting Observatory for the Study of Arctic Climate (MOSAiC) expedition from September 2019 to October 2020 (Shupe et al., 2022). Profiling the lower atmosphere with a tethered balloon system provides high resolution in situ data throughout the ABL reaching from the sea ice surface up to several hundred meters height. Those observations enable an in depth analysis of the Arctic ABL during winter and spring.

In the Arctic, the ABL is formed under unique conditions such as sea ice surface and the lack of solar radiation during winter, which favor the evolution of stable atmospheric stratification (Persson et al., 2002; Tjernström and Graversen, 2009; Morrison et al., 2012; Brooks et al., 2017). Within this study we refer to two extreme conditions typical of the Arctic ABL in winter: a cloudless boundary layer with a surface based temperature inversion, and a cloudy boundary layer with a pronounced cloud top inversion (Tjernström and Graversen, 2009; Stramler et al., 2011; Morrison et al., 2012). Under cloudless conditions, the atmosphere cools radiatively from the surface (strong negative thermal-infrared net irradiances), forming a surface based temperature inversion leading to a stably stratified lower atmosphere. Due to shear stress, the main source of turbulence in the Arctic ABL, a surface mixing layer (SML) can evolve even though stability dampens turbulence (Brooks et al., 2017). The SML is the lowermost part of the atmosphere that is turbulent or at least intermittently turbulent, however, disconnected turbulence may occur aloft (Grachev et al., 2013). If clouds form, the surface based temperature inversion is lifted upward to the cloud top. In addition to mechanically induced turbulence at the surface, a second source for turbulence at cloud top exists due to negative buoyancy, which finally leads to a cloud mixed layer (Tjernström and Graversen, 2009; Morrison et al., 2012). Especially low level Arctic clouds, impact the surface radiative energy budget (Intrieri et al., 2002a; Shupe and Intrieri, 2004) and alter the vertical structure of the ABL (Tjernström and Graversen, 2009). The stratification of the ABL influences the formation and longevity of clouds (Intrieri et al., 2002a; Sedlar and Tjernström, 2009; Shupe et al., 2013; Turner et al., 2018) as, for example, surface sources of moisture, energy and cloud forming particles are assumed to have a significant impact on cloud properties (Gierens et al., 2020; Griesche et al., 2021). While cloudless conditions are rather scarce in the Arctic (Intrieri et al., 2002b), clouds and their influence become even more important.

Furthermore, local boundary layer processes might be overlaid by advection of warmer/cooler air masses at certain altitudes. As a result, elevated inversions can form above the lowermost atmospheric layer. These elevated inversions would not meet the classical definition of the ABL, although they may well feedback to the layer near the surface (Mayfield and Fochesatto, 2013). Between the two typical states (cloudless and cloudy), the ABL alternates on the time scale of hours, but the exact time scale has not yet been investigated in detail, mostly because corresponding temporally high resolution profile measurements are missing.

Further questions include, for example, up to which height heat energy is distributed or aerosol particles are mixed from the surface. Therefore, the determination of the SML height[1] is ultimately important. The definition of the top of the SML is not

[1]We avoid the rather general term ABL height and use the term SML height for our analysis.

https://doi.org/10.5194/egusphere-2023-629
Preprint. Discussion started: 13 April 2023

always straight forward; in particular, it becomes even more complex as the criteria are not very pronounced for stable stratification (Mahrt, 1981; Stull, 1988). Here we use direct balloon borne turbulence observations, in particular, energy dissipation rate ε profiles, to estimate the SML height, which is defined as the height where turbulence ceases (Balsley et al., 2006). By observing turbulence by in situ measurements, the SML height can be either defined as the height where ε drops significantly with height, or when the flow is considered non-turbulent based on a "turbulence threshold" (Shupe et al., 2013; Brooks et al., 2017).

Other widely used approaches to determine the depth of the SML are based on observed thermodynamic profiles. An overview of common identification methods can be found in Dai et al. (2014) and Jozef et al. (2022). One approach to define the SML height applies the bulk Richardson number Ri_b (Andreas et al., 2000; Dai et al., 2014; Zhang et al., 2014; Zilitinkevich and Baklanov, 2002; Jozef et al., 2022; Peng et al., 2023). The bulk Richardson number allows the derivation of the equilibrium height where turbulence decays and from that to estimate the SML height based on a critical value (Zilitinkevich and Baklanov, 2002; Andreas et al., 2000). It should be explicitly emphasised that this approach can also be applied to a stably stratified atmosphere. The turbulence based SML heights are used to derive a critical bulk Richardson number for the wintertime and evaluate the bulk Richardson number approach. Further, continuous surface based energy flux measurements can be used to estimate the SML height using Monin-Obukhov similarity theory.

The current study discusses the observed profile measurements and the instrumental setup. Typical Arctic boundary layer properties and the effects of clouds on the vertical structure are discussed, approaches for SML height estimation for the Arctic winter and spring are examined. To investigate possible SML height criteria, the in situ energy dissipation rates are compared to bulk Richardson number profiles and a surface flux based method. Furthermore, we apply this critical value to the SML height estimation using both tethered balloon as well as radiosonde data.

2 Data and methods

2.1 Observations in the winter and spring seasons during the MOSAiC expedition

During the MOSAiC expedition, the research vessel (RV) *Polarstern* (Knust, 2017) was frozen to an ice floe following the Polar drift from October 2019 until September 2020. This expedition facilitated measurements onboard RV *Polarstern* and on the ice floe in different fields throughout an entire seasonal cycle. An overview of the atmospheric measurements is given by Shupe et al. (2022), information about the sea ice and oceanography aspects are summarized by Nicolaus et al. (2022) and Rabe et al. (2022). Figure 1a shows the course of the drift of the ship in winter and spring when the helium filled tethered balloon *Miss Piggy* was deployed from the ice floe close to RV *Polarstern*. A detailed view on the temporal evolution and the balloon flight days is given in Fig. 1b. The balloon has a volume of about 9 m^3 and allows to lift a modular scientific payload of up to 4 kg (Becker et al., 2020). The setup enables continuously vertical profiling of the lowermost 1.5 km of the atmosphere with a climbing rate of 1 to 2 $\mathrm{m\,s}^{-1}$. Measurements can be performed during day and night as well as under cloudy conditions with light icing. The deployment of the balloon is limited by weather conditions, such as strong winds or precipitation associated with severe icing. Thus, weather related selective sampling occurred and should be considered for further interpretation.

https://doi.org/10.5194/egusphere-2023-629
Preprint. Discussion started: 13 April 2023

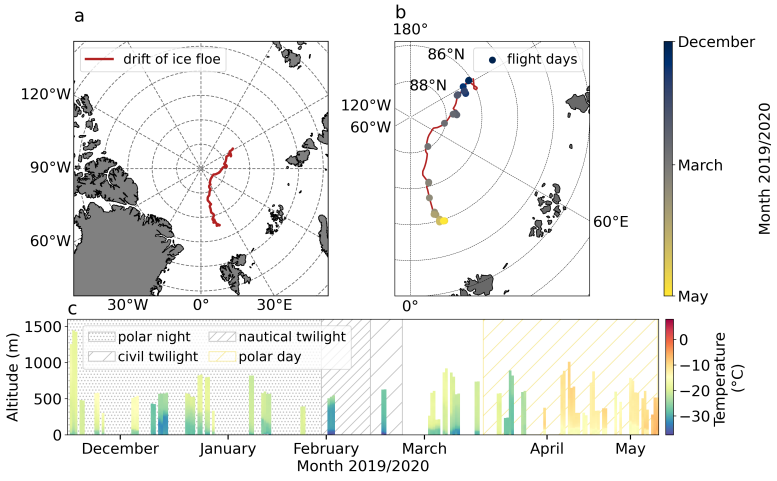

Figure 1. Overview of the drift of the ice floe during tethered balloon operations in winter and spring (a), daylight conditions and location of the days with balloon operations (b). Temperature measurements of all profiles is shown in (c). The background shading indicates the respective daylight conditions during the observation period.

The data used in this work were measured with a hot wire anemometer package specifically designed for turbulence observations (Egerer et al., 2019) drifting between 86.14 °N 122.21 °E and 83.92 °N 17.69 °E between 6 December 2019 and 6 May 2020 (Fig. 1b). The instrument is attached to a tether about 10 m below the balloon to minimize flow distortions induced by the balloon. The system is mounted movably, aligned horizontally and equipped with a tail to keep the setup into the mean flow direction. The instrument consists of an one component hot wire anemometer to measure wind velocity and a thermocouple for air temperature observations with 125 Hz temporal resolution. Besides the high frequency records, 1 Hz measurements of wind velocity based on a Pitot static tube are available accompanied by basic measurements of static pressure, temperature, and relative humidity. Due to weather conditions, the Pitot tube, which served as a reference for hot wire calibration, was frequently affected by icing. Therefore, a standard meteorology tethersonde, which is part of the modular balloon equipment and separated approximately 5 m from the turbulence probe, served as mean reference for the fast sensors. The turbulence probe was deployed on 34 days reaching from the surface up to typically a few hundreds meters. After quality control, 88 individual vertical profiles (ascents and descents) are available for further analysis. Figure 1c displays an overview of all temperature profiles, the respective maximum height and daylight conditions.

Continuous observations of meteorological and turbulence parameters were performed at a location on the ice floe called *Met City* (Shupe et al., 2022). Measurements with an ultrasonic anemometer/thermometer were taken at a meteorological tower in 2 m, 6 m, and 10 m height serving as surface reference for our balloon observations. Furthermore, the net irradiances are taken as a proxy for the radiative energy budget at the surface. Regular radiosondes were launched every six hours (5, 11, 17, and 23 UTC) from the helicopter deck of RV *Polarstern* (12 m above mean sea level) providing information on the thermodynamic structure of the atmosphere. It should be noted, however, that the data obtained within the first tens of meters can be influenced

https://doi.org/10.5194/egusphere-2023-629
Preprint. Discussion started: 13 April 2023

by the ship itself and should therefore be interpreted with caution. The ship can create flow distortions and can serve as a heat island, but also radiosonde data near the surface are often still subject to errors. Especially the wind determined by GPS data might be influenced by the unwinding of the probe from the tether (Achtert et al., 2015; Jozef et al., 2022). To compare the radiosonde to the tethered balloon profiles, the corresponding radiosonde measurements are selected with launch times closest to the tethered balloon flight. The time difference between both launches is at most around 3 hours. However, the atmospheric structure may change within a few hours or even less. The evolution of the atmosphere has to be considered when comparing the respective launches.

In situ measurements are complemented by Cloudnet retrievals to characterize the cloud situation (Illingworth et al., 2007; Griesche et al., 2020). The cloudy Arctic ABL can be very shallow, especially in winter, and hence poses challenges on remote sensing approaches to detect the very low cloud layers (Griesche et al., 2020). For the question of the influence of clouds on the ABL dynamics, however, the net radiation is of importance, which is directly influenced by the clouds. Therefore, the net radiation (F_{net}) measurements at *Met City*, where F_{net} is the cumulative surface radiative flux, are used as an independent "cloud indicator". Cloudless conditions prevail when the net radiation is below -25 W m^{-2}, while higher values are associated with clouds. To avoid ambiguous allocations, data with net radiation in the range between -28 W m^{-2} and -22 W m^{-2} are not considered.

2.2 Estimation of the surface mixing layer height

The determination of the SML height can be done in different ways depending on the type of measurements available. A comprehensive overview of the different methods is given by Vickers and Mahrt (2004). Here we focus mainly on the advantage of high resolution profile measurements using the tethered balloon. Thus, we first discuss a method that benefits directly from local turbulence measurements and then, serves as a reference for a method based on mean profiles. Finally, we compare the results with a method based on surface flux observations.

2.2.1 In situ turbulence method

The basic idea behind the definition of a SML height is that starting from the surface, a property or matter is mixed by turbulence upwards, and this mixing is terminated when the turbulence is no longer strong enough for vertical mixing. An obvious definition of the SML height h is, therefore, based on the vertical distribution of a suitable turbulence parameter and a threshold, which, if below this value, defines the SML height (Dai et al., 2014).

For our application, we chose the energy dissipation rate ε as turbulence measure because it can be determined as a local parameter from short temporal subsections during a balloon ascent. Based on Kolmogorov's inertial subrange theory, ε can be estimated in different ways (Wyngaard, 2012). A comparatively robust method has been found to determine ε using the second-order structure function (Siebert et al., 2006, and references therein):

$$S^{(2)}(\tau) = \left\langle (u(t+\tau) - u(t))^2 \right\rangle = 2(\varepsilon \cdot U \cdot \tau)^{2/3}, \quad (1)$$

https://doi.org/10.5194/egusphere-2023-629
Preprint. Discussion started: 13 April 2023

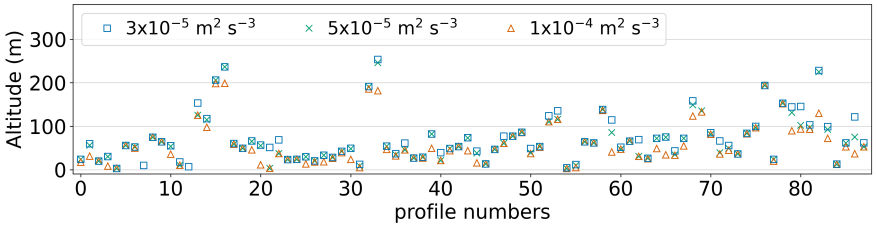

Figure 2. Surface mixing layer heights derived from direct turbulence measurements for each profile. Three thresholds separate turbulent and non-turbulent flows: 1x10^{-4} m^2 s^{-3}, 5x10^{-5} m^2 s^{-3}, and 3x10^{-5} m^2 s^{-3}.

with $u(t)$ being the longitudinal wind velocity component as measured at time t. The averaging in Eq. (1) denoted by the rectangular brackets is performed over all t, so the structure function $S^{(2)}$ is a function of time lag τ which has been calculated by applying Taylor hypothesis ($r = U \cdot \tau$) with the mean flow velocity U. It has been shown by Frehlich et al. (2003) that 100 samples are sufficient in order to provide robust estimates of local ε. Here, we use an integration over 125 samples (e.g., 1 s) resulting in a vertical resolution of roughly 2 m.

Therefore, profiles of ε allow direct identification of the SML height, denoted hereafter as h_ε. This method has the disadvantage that there is no physically unambiguous definition of the limit value for ε and therefore different values are used in the literature (Shupe et al., 2013; Brooks et al., 2017), which are close to each other. We tested three values to estimate h_ε that previously have been used: 1x10^{-4} m^2 s^{-3}, 5x10^{-5} m^2 s^{-3} and 3x10^{-5} m^2 s^{-3}. We consider the SML to be constrained when ε falls below the threshold for 10 consecutive levels while the h_ε equals the lowermost of those 10 consecutive levels.

Figure 2 shows the different estimates of h_ε for each profile depending on the different thresholds. Although the highest threshold almost always results in the lowest h_ε values, the variations for the different thresholds vary considerably from profile to profile. However, the two lowest thresholds are very close to each other and result in almost identical h_ε. To identify the appropriate threshold value, we have manually examined the thermodynamic profiles and the profiles of the ε. As a result we have decided on the threshold value of ε = 3x10^{-5} m^2 s^{-3}.

2.2.2 Bulk Richardson number method

The turbulent state of an atmospheric layer can be analyzed using the (gradient) Richardson number Ri, which describes the relationship between thermodynamic stability and turbulence producing wind shear (e.g., Stull, 1988):

$$\mathrm{Ri_g(z)} = \frac{\frac{g}{\theta}\frac{\partial \theta}{\partial z}}{(\frac{\partial u}{\partial z})^2 + (\frac{\partial v^2}{\partial z})^2}, \tag{2}$$

with the potential temperature θ, the horizontal wind components u and v (zonal and meridional, respectively), and the gravitational acceleration g = 9.81 m s^{-1}. This stability measure describes whether there is a tendency for turbulence to weaken or strengthen, usually a theoretical value of 0.25 is assumed at which the tendency turns. Therefore, Ri profiles can be used to derive the equilibrium height at which turbulence decays which coincides with the SML height (Zilitinkevich and Baklanov,

https://doi.org/10.5194/egusphere-2023-629
Preprint. Discussion started: 13 April 2023

2002; Andreas et al., 2000). However, the practical use of the gradient Ri is somewhat limited because the calculation of mean gradients (temperature and wind speed) based on observational data is often subject to uncertainties that lead to large variations in the Ri profiles, and, the necessary filtering leads to further ambiguities. For this reason, modified definitions for Ri have been derived, which offer advantages especially for observational data. An alternative Ri number is the so called surface bulk Richardson number Ri_{b} (Mahrt, 1981; Andreas et al., 2000; Heinemann and Rose, 1990) whose definition is not based on the explicit calculation of local gradients, but includes the complete layer from the ground to the current measurement height z:

$$\mathrm{Ri_b(z)} = \frac{gz\frac{\Delta\theta}{\theta_0}}{(U(z))^2}, \tag{3}$$

with the numerator as the buoyancy term, where θ_0 is the potential temperature at the surface level, $\Delta\theta = \theta(z) - \theta_0$ is the difference between the potential temperatures at the current height z and the surface level, and g is the gravitational acceleration. $U(z)$ is the horizontal wind speed at height z indicating the bulk shear. For surface temperature, we use observations at the 2 m height of the *Met City* tower, because the balloon borne temperature readings are not completely reliable within the lowest meters. Surface bulk Richardson numbers are calculated for each altitude z of the profile with the surface as lower level assuming that the wind velocity at the surface vanishes. Compared to other bulk Ri-definitions where mean gradients are estimated for distinct layers of δz (Jozef et al., 2022), the surface Ri-approach applied here fails if multiple turbulent layers are present. However, as we want to estimate the height of the SML, detecting only the lowermost continuous turbulent layer is needed and the surface approach with an increasing layer depth is sufficient. Furthermore, looking at h_ε in Fig. 2, it is apparent that the majority of the SML heights lies within the lowermost 100 m, many even do not exceed 50 m altitude and multi turbulence layers are rare.

The height of the SML $h_{Ri_{\mathrm{b}}}$ can be defined as the altitude where a critical value of the bulk Richardson number Ri_{bc} is reached and turbulence decays. The top of the SML is the highest level where $Ri_{\mathrm{b}} < Ri_{\mathrm{bc}}$. The definition of Ri_{bc} is, however, not straightforward and a variety of Ri_{bc} values can be found in literature (e.g., Zilitinkevich and Baklanov, 2002). It appears that the differences for Ri_{bc} measured at different sites are larger than the variation within an observation period at a fixed site (Vickers and Mahrt, 2004) and the "theoretical value" of $Ri_{\mathrm{bc}} = 0.25$ overestimates the experimentally determined values (Brooks et al., 2017). However, it must be taken into account that the theoretical value was derived for the gradient Ri number and, therefore, it is not directly applicable to the surface bulk approach. However, by comparison with the "reference" SML height h_ε introduced in subsection 2.2.1 Ri_{bc} can be estimated (see Sec. 3.3).

2.2.3 Surface flux based method

If surface fluxes dominate the development of a SML, the height h_{sf} should be a function of the Monin-Obukhov length L (Vickers and Mahrt, 2004):

$$L = -\frac{u_\star^3}{B_s}, \tag{4}$$

https://doi.org/10.5194/egusphere-2023-629
Preprint. Discussion started: 13 April 2023

with $B_s = g{T_0}^{-1} \langle w'T' \rangle$ being the normalized surface buoyancy flux and $u_\star^2 = -\langle u'w' \rangle$ being the friction velocity. Besides more simple relationships ($h_{\mathrm{sf}} \propto L$, Kitaigorodskii, 1960), Zilitinkevich (1972) proposed a formulation including the Earth's rotation:

$$h_{sf} = C_{sr} \sqrt{\frac{u_\star L}{f}}, \tag{5}$$

with C_{sr} being a scaling constant of $\mathcal{O}(1)$ and the Coriolis parameter f. All parameters included in Eq. (5) have been calculated continuously using ultrasonic anemometer readings at the *Met City* tower. However, Eq. (5) is only valid for stable stratification ($B_{\mathrm{s}} < 0$ and $L > 0$) and the method fails if further sources for turbulence are present at higher levels.

3 Results and discussion

3.1 Two contrasting states of the Arctic wintertime ABL: surface based versus elevated inversion

In the introduction (Sect. 1), it was argued that the Arctic winter ABL alternates between two cloudless and cloudy conditions. We begin at this point by illustrating these two typical conditions with the help of examples. The first case represents a cloudless ABL with a pronounced surface inversion, and the second case describes a cloudy ABL and the resulting elevated inversion at the cloud top with a less well mixed, neutrally stratified layer below the inversion. Figure 3 shows the two example measurements of potential temperature θ, horizontal wind velocity U, local energy dissipation rate ε, and surface bulk Richardson number Ri_{b} as function of altitude. Cloudless conditions prevailed during a profile observed on 5 March 2020 with a strong surface based temperature inversion ($\Delta\theta \approx 6\,\mathrm{K}$ within 40 m) up to 50 m followed by a slightly stably stratified layer above (Fig. 3a). Near the surface, the wind speed increases with height, peaking at about 50 m again and continuing almost constantly until the maximum height of the profile (Fig. 3b). The strongest increase in wind speed is in the lowest altitude layers up to about 30 m, in the region with the strongest turbulence in terms of ε (Fig. 3c). Above 30 m, the turbulence decreases rapidly by two to three orders of magnitude and according to the threshold, as defined in Sect. 2.2.1, the upper limit of the SML height is reached here.

The surface bulk Richardson number (Fig. 3d) almost linearly increases with height for the cloudless conditions. The example for the vertical stratification under cloudy conditions as measured on 29 December 2019 indicates an elevated inversion with its base at around 220 m indicating cloud top. A well mixed layer prevails below the inversion with the wind speed gradually increasing from the surface to the inversion base from $6\,\mathrm{m\,s^{-1}}$ to $9\,\mathrm{m\,s^{-1}}$. Clearly, the turbulence reaches from the surface up to around 240 m height where it rapidly drops below the threshold indicating the height of the SML. The extent of the mixing layer is also clearly visible in the Ri_{b} profile (Fig. 3d). The surface bulk Richardson number is almost constant in height in this region with values close to zero and starts to significantly grow only at the inversion base height exactly where ε starts to decrease almost abruptly and the upper limit of the SML height is reached.

https://doi.org/10.5194/egusphere-2023-629
Preprint. Discussion started: 13 April 2023

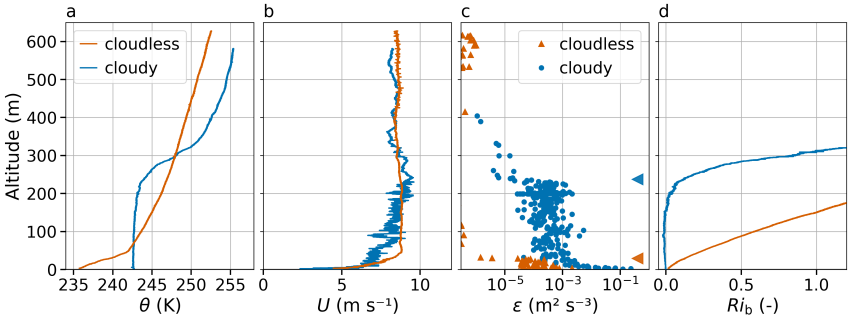

Figure 3. Tethered balloon borne profiles obtained under cloudless conditions (orange) on 5 March 2020, 12:29 UTC, and under cloudy conditions (blue) on 29 December 2019, 11:56 UTC. Panel (a) shows the profiles of potential temperature over height, (b) the respective wind velocity, (c) the derived energy dissipation rates and (d) the bulk Richardson number. The SML heights derived by in situ turbulence records are indicated by triangles in (c).

3.2 Vertical mean and turbulent structure of the ABL

To obtain the typical features of the mean temperature stratification for the two typical situations, we normalize all measured profiles and plot and average them (Fig. 4), distinguished between surface (Fig. 4a) and elevated (Fig. 4b) inversions. The height is normalized by h_ε and the temperature is shifted by the surface value θ_0 and normalized by the inversion strength ($\Delta\theta = \theta(h_\varepsilon) - \theta_0$) so that the normalized temperature in the SML height takes the value one. A similar plot including the contrasting summertime Arctic can be found in Tjernström and Graversen (2009).

Due to operational constraints, not all profiles reach up to the same height but every launch exceeds 200 m altitude and, therefore, most of the profiles exceeds at least twice h_ε. The two averaged temperature profiles have quite different characteristics. While the profile is nearly linear from the ground to h_ε under cloudless conditions, the well mixed sub cloud layer for the cloudy case provides a gradual increase in temperature to then rise much more sharply when h_ε is reached. As it is often observed in Arctic clouds, the temperature rise at inversion base already begins clearly inside the cloud; in this normalization, the cloud layer thickness is not included and, hence, the temperature curve in Fig. 4b must be interpreted with caution. In addition, it must be emphasized that we do not present the liquid water potential temperature, which under adiabatic conditions is also height constant within the cloud.

In Fig. 5 the relative probability distribution of ε is shown using 5 m height intervals of all measured profiles. The turbulence distribution for surface based inversions (Fig. 5a) shows highest values near surface (wind shear driven turbulence) and significantly low values above approximately 60 m height. Higher probabilities of ε at heights around 500 m occurred during single events and might be related to Low-Level Jets (LLJ). However, the observations are too sparse to draw conclusions about the occurrence of possible multi layer turbulent structures. For ABL structures with elevated inversions, the turbulence is still highest in the lowermost tens of meters. But here, the turbulence continuously reaches up to around 200 m. The chosen threshold of ε = 3x10^{-5} m^2 s^{-3} is used to distinguish turbulent and non-turbulent regions of the profiles. Using this threshold

https://doi.org/10.5194/egusphere-2023-629
Preprint. Discussion started: 13 April 2023

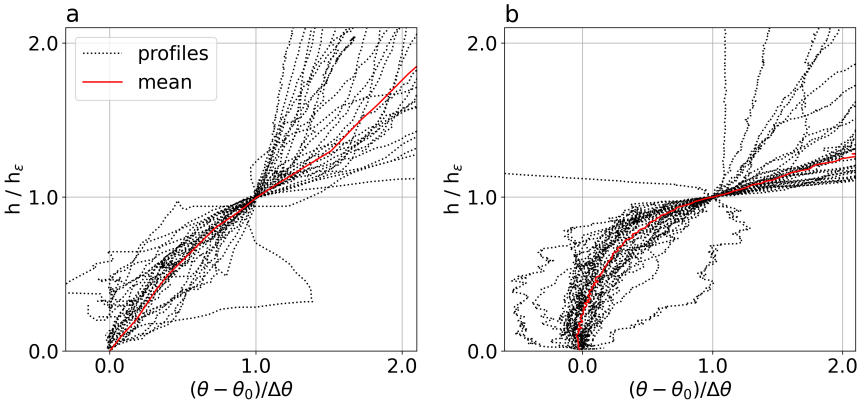

Figure 4. Normalized potential temperature profiles of tethered balloon borne measurements over height. All profiles are separated in respect to the inversion heights, such as surface based inversion (a) or elevated inversion (b). The height is normalized using the turbulence based SML height h_ε while the temperature is normalized using the potential temperature gradient of the SML and the potential temperature close to the surface.

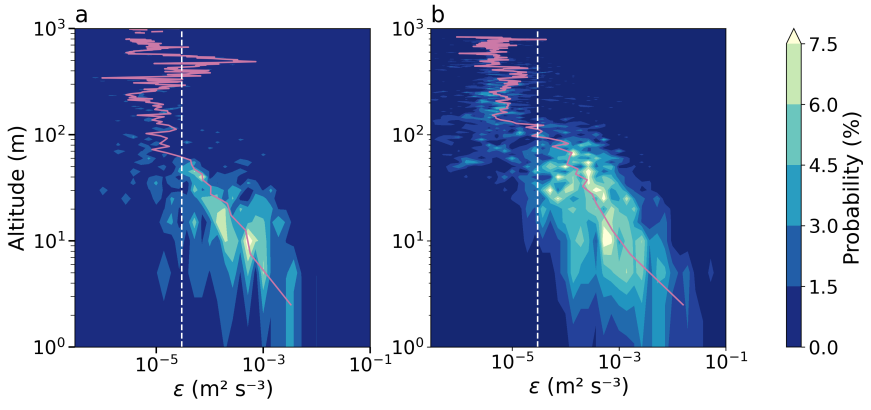

Figure 5. Probability of the energy dissipation rates as a function of height. The profiles are distinguished in respect to the temperature profile: (a) shows all profiles with surface based inversions and (b) profiles with elevated inversions. The probability of ε is calculated for 5 m height bins. Additionally, the median (solid line) profile of ε (5 m bins) is given in purple, respectively. The turbulence threshold value of $3\text{x}10^{-5}$ m^2 s^{-3} is depicted by the white vertical dashed line in both panels.

approach, almost all observations above 200 m height for elevated inversions (60 m height for surface inversions) are considered as non-turbulent and, therefore, well above the SML. In contrast to the summertime Arctic boundary layer where Brooks et al. (2017) found two separated turbulence maxima indicating decoupling, we did not identify clearly pronounced turbulence layering and decoupling plays a minor role.

https://doi.org/10.5194/egusphere-2023-629
Preprint. Discussion started: 13 April 2023

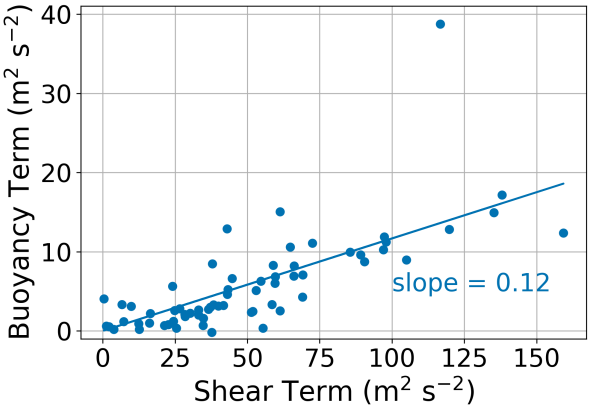

Figure 6. The buoyancy term versus shear term of the surface bulk Richardson number calculated according to Eq. 3. The solid line indicates the least squares fit that is forced through the origin. The critical bulk Richardson number Ri_{bc} is equivalent to the slope of the fit: 0.12.

3.3 Estimating the critical Bulk Richardson Number

The estimation of the SML height based on the surface bulk Richardson number requires the definition of the critical value Ri_{bc}. Here, we apply a method used by Vickers and Mahrt (2004) by plotting the buoyancy term versus the shear term in Fig. 6 for all profiles at h_{ε}. The slope of the linear fit is then equivalent to the critical surface bulk Richardson number Ri_{bc}. Based on a data set comprising 64 profiles, we derive a critical value of $Ri_{\mathrm{bc}} = 0.12$ which is about half of the theoretical value 0.25.

In order to get a rough measure for the robustness of the Ri_{bc} estimate, Fig. 7a shows the frequency of occurrence of Ri_{bc}. Clearly, the majority of Ri_{bc} is centered around the mean value of 0.12 ± 0.04 with a few outliers even exceeding the theoretical value.

As described by Vickers and Mahrt (2004), the critical bulk Richardson number varies not only between locations but also under different atmospheric conditions (cloudless, cloudy). To understand which influence might lead to different Ri_{bc}, the data are separated according to the cloud conditions because the radiative effect of clouds directly changes the turbulent fluxes at surface and thus the SML height. Figure 7b shows the distribution of Ri_{bc} for cloudless and cloudy conditions, respectively. Even though the frequency distribution of Ri_{bc} for cloudless conditions peaks at slightly higher values than for cloudy conditions, the differences for the two mean case depending Ri_{bc} is below 1% and therefore negligible and the mean value of 0.12 is used for all conditions.

3.4 Surface mixing layer height estimates based on a mean critical Richardson number

To assess the impact of using an averaged critical Ri number on the determination of the individual SML height, we compare $h_{\mathrm{Ri_b}}$ to the turbulence based h_{ε}. In addition to the tethered balloon profiles, we apply the same surface bulk Richardson number method to the radiosondes profiles using the *Met City* tower data as surface reference. Figure 8 shows the comparison of the

https://doi.org/10.5194/egusphere-2023-629
Preprint. Discussion started: 13 April 2023

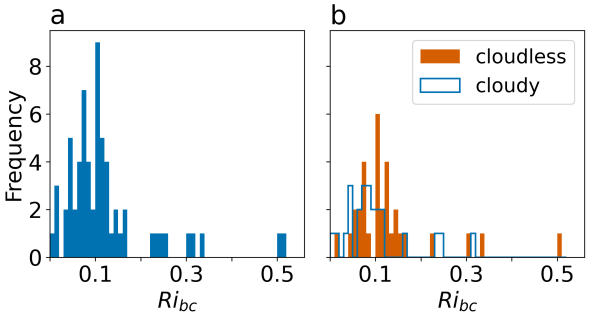

Figure 7. Frequency distributions of bulk Richardson numbers at the SML height h_ε for (a) all tethered balloon profiles, and (b) for cloudless and cloudy conditions, respectively.

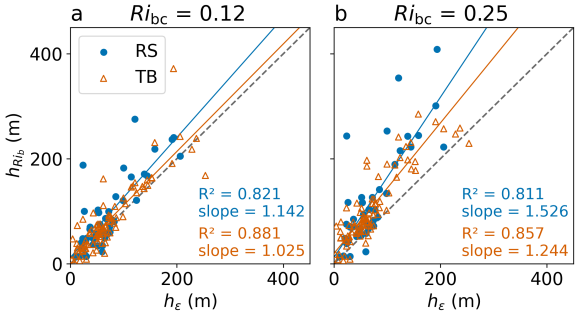

Figure 8. SML height comparisons between the bulk Richardson number approach $h_{\mathrm{Ri_b}}$ and turbulence h_ε based on tethered balloon (TB, orange) and radiosonde (RS, blue) profiles. For both data sets, two different critical bulk Richardson numbers are used: 0.12 (a), and 0.25 (b). The dashed line represents the 1:1 line. Solid lines represent the least squares fit for tethered balloon (orange) and radiosonde (blue) profiles; R^2 and slope values are given for each fit.

mixing layer heights applying two different Ri_{bc} for both, tethered balloon borne as well as radiosonde profiles. We use those radiosonde profiles that were launched closest to the tethered balloon flight. In the scatter plots the solid lines are the least squares fits (linear regressions) correspondingly; the statistical measure R^2 (coefficient of determination) and the slope of the fit are printed in the according color. In the tethered balloon observations, the slope, and thus h, using the theoretical value of 0.25 is about 20 % higher than when using $Ri_{\mathrm{bc}} = 0.12$ supporting the need of an accurate estimate of Ri_{bc}. If we apply the newly determined Ri_{bc}, and the theoretical value for comparison, to the radiosonde observations the inaccuracies in the determination of h become even more apparent. It should be noted that the reference altitude h_ε was not determined exactly at the same time as the height based on the radiosonde ascents.

In a final step, we use $Ri_{\mathrm{bc}} = 0.12$ to derive h for all radiosonde launches collected during winter and spring. The time series of the derived SML height is shown in Fig. 9. Additionally, h_ε of the tethered balloon borne turbulence estimates are displayed. In Fig. 9 a high variability of the SML height is displayed during the entire observation period, reaching from a few tens of meters up to 600 m and more (maximum 925 m). It has to be considered that the minimum detection limit of the radiosonde

https://doi.org/10.5194/egusphere-2023-629
Preprint. Discussion started: 13 April 2023

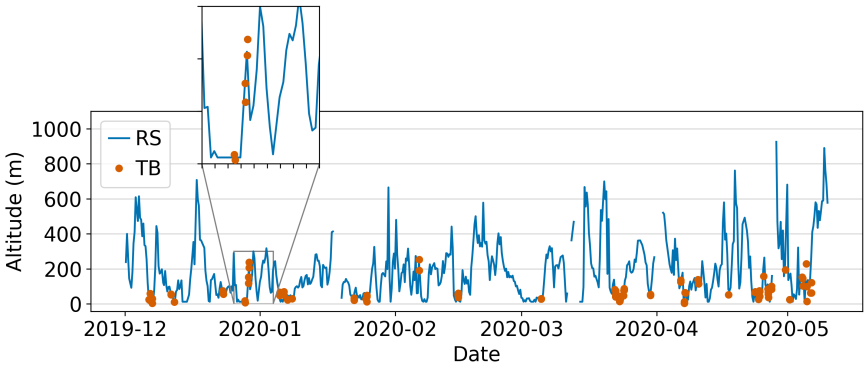

Figure 9. Time series of SML heights from radiosonde data derived with bulk Richardson number method using $Ri_{\mathrm{bc}} = 0.12$. The time series of radiosonde launches is displayed between 1 December 2019 and 10 May 2020 (blue). Additionally, the SML heights h_ε of tethered balloon borne profiles are shown as orange dots.

is of about 12 m due to launching from the helicopter deck. A significant growth of the SML is likely related to weather or storm events while the SML is shallower for calm or stable conditions. The vast majority (around 81 %) of the SML heights derived from the radiosondes during this period is below 300 m and around half of the profiles lead to a SML height smaller than 150 m. That shows that even if measurements with the tethered balloon are limited by weather conditions, the balloon measurements can still represent a large part of the SML in this season/time of the year.

Frequency distributions of all derived SML heights using radiosonde data are shown in Fig. 10. During this period the majority of all SML heights is clearly below 250 m (Fig. 10a). Separating between cloudless and cloudy conditions shows that SML heights are spread rather equally between all heights for cloudy conditions, but are significantly smaller for cloudless conditions (Fig. 10b). During daylight conditions (Fig. 10c and d), less cloudless profiles are measured but the distribution is similar, however, the number of profiles with daylight is smaller than during night conditions for our period of analysis. Distributions of the SML heights during polar night are shown in Fig. 10e for all conditions, and separately in Fig. 10f. We see that the majority of cloudless conditions lead to SML heights of maximum 100 to 200 m, while cloudy conditions do not show any tendency towards a distinct SML height. This shows the variety of clouds and their respective influence on the SML.

3.5 Surface mixing layer height estimates based on Monin-Obhukov scaling

Under stable conditions ($B_\mathrm{s} < 0$ and $L > 0$), we apply the surface flux based alternative method introduced in Sect. 2.2.3 to determine the mixing layer height h_MO based on Monin-Obukhov (MO) similarity. The two covariances underlying the definition of L are estimated from ultrasonic anemometer/thermometer observations from the *Met City* tower in 2 m height. A running average ($\tilde{x}(t)$) with a centered window over 5 minutes is applied to define the time series of the fluctuating part as $x'(t) = x(t) - \tilde{x}(t)$ where $\langle x'(t) \rangle = 0$ is fulfilled and x is one of the velocity components (u, v, w) or virtual temperature T_v (actually, an ultrasonic thermometer measures the so called "sonic temperature" which differs only very slightly from the virtual temperature at the low humidifies), respectively. The averaging to calculate the kinematic fluxes leading to L and, finally

https://doi.org/10.5194/egusphere-2023-629
Preprint. Discussion started: 13 April 2023

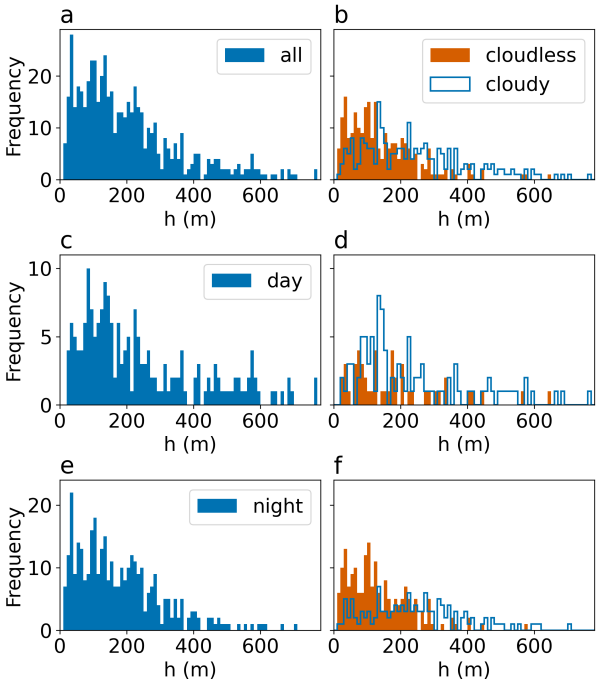

Figure 10. Frequency distribution of SML heights using radiosonde data between 1 December 2019 and 10 May 2020. The radiosonde SML heights are based on bulk Richardson number approach with $Ri_{\mathrm{bc}} = 0.12$. The frequency distributions are given for (a) all radiosonde profiles, (b) all data separated according to cloud conditions, (c) all profiles with daylight conditions and (e) all profiles during night, (d) and (f) show the cloudless and cloudy conditions, respectively.

to h_{MO} is done over 30 minutes centered around the balloon ascents/descents. Figure 11 shows the time series of h_{MO} (Fig. 11a) including h_ε as reference and the Monin-Obukhov length L (Fig.11b). The net radiation F_{net} is shown in (Fig.11c), a threshold of $-25\,\mathrm{W\,m^{-2}}$ separates cloudless from cloudy conditions.

Figure 11 shows that for cases with two or more subsequent values with $F_{\mathrm{net}} < -25\,\mathrm{W\,m^{-2}}$, which cover longer lasting cloudless cases, there is a high qualitatively agreement between h_{MO} and h_ε. This holds particular true for the polar night and twilight periods. In contrast, for 29 December 2019 (profile numbers 13 to 16 in Fig. 11, cf. Fig. 3), we find $F_{\mathrm{net}} > -25\,\mathrm{W\,m^{-2}}$ describing a more cloudy situation with increasing F_{net}. At the beginning of this cloudy period, we find a reasonable agreement between h_{MO} and h_ε but eventually, with further increasing F_{net}, L becomes negative and MO theory fails to predict a SML height. Therefore, in situations with rapidly changing cloud cover, SML determinations using MO theory are only partially successful and F_{net} observations can at least indicate these possible problems if no vertical profiles are available.

During a short period on 6 February 2020 with two profiles (32 and 33), a situation with obvious disagreement between h_{MO} and h_ε but $F_{\mathrm{net}} < -25\,\mathrm{W\,m^{-2}}$ and L being positive has been identified. This cloudless period was influenced by a LLJ adding

https://doi.org/10.5194/egusphere-2023-629
Preprint. Discussion started: 13 April 2023

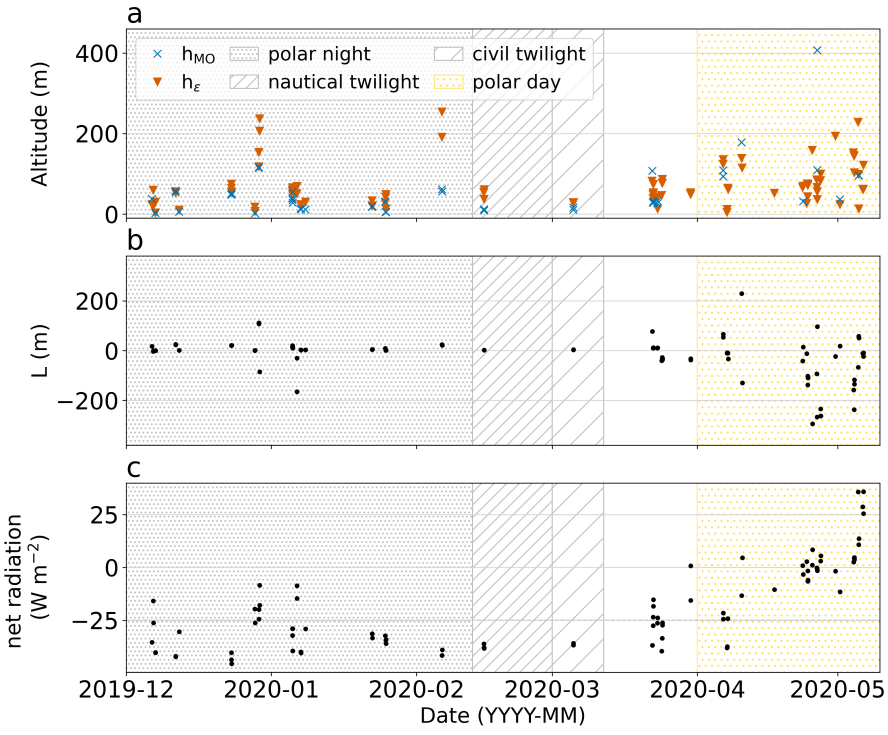

Figure 11. SML heights (a) estimated based on MO (h_{MO}) and energy dissipation rate (h_ε) as a function of profile number, (b) Monin-Obukhov length L, and (c) the net radiation F_{net} as observed at surface. The periods in terms of daylight conditions are given for reference.

a further source of turbulent kinetic energy well above the surface. The resulting profile of ε, therefore, never falls below the threshold for h_ε between the core of the LLJ and the surface suggesting a SML height much higher compared to h_{MO}.

In the context of clouds, there is another special situation that can be misinterpreted. Shallow ground fog within a neutrally layered SML up to about $45\,\mathrm{m}$, capped by an inversion as observed in late March (profile number 46 to 51). The fog was optically quite thin, associated with F_{net} around $-25\,\mathrm{W\,m^{-2}}$. Due to the elevated inversion, the turbulence threshold value was reached below $100\,\mathrm{m}$. MO theory failed to predict a SML height because $L < 0$.

With beginning of the twilight (15 February 2020, profile numbers 34 to 36), the cloudless ABL was characterized by a surface inversion and a second elevated inversion above with a weakly stable to neutral stratified layer in between. Below the elevated inversion, ε was always slightly above the threshold for h_ε suggesting at least some vertical turbulent mixing. However, h_{MO} significantly underestimates the SML height under those conditions.

The situation becomes even more complicated in the transition to polar day when the thermal stratification changes from rather stable to neutral or unstable, and the cloud situation - even with some foggy days - often becomes very complex. This becomes especially clear at the end of the observation period when L is often negative and thus no SML height can be determined based on MO theory.

https://doi.org/10.5194/egusphere-2023-629
Preprint. Discussion started: 13 April 2023

4 Summary and conclusion

This work investigates methods to determine the SML height under different ABL conditions as observed during wintertime and early spring in the central Arctic during MOSAiC. The quantitative identification of the SML height is of considerable significance with regard to the vertical distribution of aerosol particles, clouds and trace gases, as well as cloud formation and decay and precipitation and energy flux processes. For our analysis we have used tethered balloon borne profile measurements of mean and turbulence parameters accompanied by radiosondes and tower based turbulence observations.

Two typical cases - cloudless with a surface inversion and cloudy with a capping inversion at the cloud top - were observed and analyzed in detail. Our turbulence measurements allowed direct estimates of the SML height based on a turbulence threshold that is independent of assumptions on stratification or sources of the turbulent mixing. With help of this reference height, the surface bulk Richardson number method was applied and the critical Ri_{bc}, necessary for further SML height estimates, was derived for the conditions observed during winter and spring of MOSAiC.

It was found that differences in Ri_{bc} for cloudless and cloudy conditions can be neglected and a common value of $Ri_{\mathrm{bc}} = 0.12$ can be recommended under most conditions. Using the Ri_{b} method and the Ri_{bc} value determined in this work, regular radiosonde ascents provide reliable estimates of the SML when direct determinations using turbulence profiles are not available. Finally, another method for SML height determination based on near surface turbulent fluxes (Monin-Obukhov method) was compared to the reference method and its limitations were investigated.

All methods have advantages and disadvantages. We conclude that without extensive vertical measurements of both mean and turbulent parameters, limitations in some methods may not be detected at all. This leads to the following specific conclusions:

There is some confusion in literature about the observed variability of Ri_{bc}, which is probably caused by the usage of different definitions of Ri, such as the classical gradient Ri number versus the different bulk approaches. It was argued that the critical values vary less within an experiment than between different experiments. Since we did not find a significant difference in Ri_{bc} for cloudless and cloudy conditions, this hints to the different methods as the main cause of this issue. Therefore, values taken from the literature should always be interpreted taking into account the specifics of the approach applied. Turbulence profiles are eminent in determining Ri_{bc} and should serve as a reference for determining the height of the SML.

Under certain conditions Monin-Obukhov theory provides reliable SML heights. However, if only turbulence measurements at the surface are available phenomena such as LLJ cannot be unambiguously detected. Here, at least radiosondes are essential for an assessment. It should be noted that in the Arctic the occurrence of LLJs is very common (López-García et al., 2022).

In our study, the time resolution of the profiling was insufficient to study the important transition processes between cloudless and cloudy conditions. The question remains, how quickly the SML height changes during the polar night when clouds move in or whether those processes are related to local forcing or advection.

https://doi.org/10.5194/egusphere-2023-629
Preprint. Discussion started: 13 April 2023

Data availability. All tethered balloon borne data and radiosonde data are available on PANGAEA (Akansu et al., 2021, 2022; Maturilli et al., 2022). Surface based tower measurements are available on the Arctic Data Center (Cox et al., 2021) and Cloudnet data (CLU, 2023) can be found here: https://hdl.handle.net/21.12132/2.b697d787e83344ce.

Author contributions. H.S. designed the turbulence probe. H.S., S.D., and M.W. contributed to the data analysis and scientific discussion. E.A. processed the data and prepared the manuscript.

Competing interests. The authors declare that they have no conflict of interest.

Acknowledgements. We gratefully acknowledge the funding by the Deutsche Forschungsgemeinschaft (DFG, German Research Foundation) – project number 268020496 – TRR 172, within the Transregional Collaborative Research Center "ArctiC Amplification: Climate Relevant Atmospheric and SurfaCe Processes, and Feedback Mechanisms (AC)3 " in sub project A02. Data used in this manuscript were produced as part of the international Multidisciplinary drifting Observatory for the Study of the Arctic Climate (MOSAiC) with the tag MOSAiC20192020 and the Project_ID: AWI_PS122_01, AWI_PS122_02, AWI_PS122_03. Here, our special thanks go to A. Sommerfeld, J. Gräser and R. Jaiser from the Alfred Wegener Institute who performed the balloon measurements during the first three legs. Tower based measurements were made by the University of Colorado / NOAA surface flux team supported by National Science Foundation (OPP-1724551). Surface radiation measurements were provided by the Atmospheric Radiation Measurement (ARM) User Facility, a U.S. Department of Energy (DOE) Office of Science User Facility Managed by the Biological and Environmental Research Program. Finally, we thank O. Persson and M. Shupe for fruitful and stimulating discussions on the Arctic atmospheric boundary layer.

https://doi.org/10.5194/egusphere-2023-629
Preprint. Discussion started: 13 April 2023

References

Achtert, P., Brooks, I. M., Brooks, B. J., Moat, B. I., Prytherch, J., Persson, P. O. G., and Tjernström, M.: Measurement of wind profiles by motion-stabilised ship-borne Doppler lidar, Atmos. Meas. Tech., 8, 4993–5007, https://doi.org/10.5194/amt-8-4993-2015, 2015.

Akansu, E. F., Siebert, H., Dahlke, S., Graeser, J., Jaiser, R., and Sommerfeld, A.: Tethered balloon-borne measurements of turbulence during the MOSAiC expedition from December 2019 to May 2020, PANGAEA, https://doi.org/10.1594/PANGAEA.932007, 2021.

Akansu, E. F., Siebert, H., Dahlke, S., Graeser, J., Jaiser, R., and Sommerfeld, A.: Energy dissipation rate profiles derived from tethered balloon-borne measurements during the MOSAiC expedition from December 2019 to May 2020, PANGAEA, https://doi.pangaea.de/10.1594/PANGAEA.948546, 2022.

Andreas, E. L., Claffy, K. J., and Makshtas, A. P.: Low-Level Atmospheric Jets And Inversions Over The Western Weddell Sea, Boundary Layer Meteorol., 97, 459–486, https://doi.org/10.1023/A:1002793831076, 2000.

Balsley, B. B., Frehlich, R. G., Jensen, M. L., and Meillier, Y.: High-Resolution In Situ Profiling through the Stable Boundary Layer: Examination of the SBL Top in Terms of Minimum Shear, Maximum Stratification, and Turbulence Decrease, J. Atmos. Sci., 63, 1291–1307, https://doi.org/10.1175/JAS3671.1, 2006.

Becker, R., Maturilli, M., Philipona, R., and Behrens, K.: In situ sounding of radiative flux profiles through the Arctic lower troposphere, Bull. of Atmos. Sci.& Technol., 1, 155–177, https://doi.org/10.1007/s42865-020-00011-8, 2020.

Bintanja, R., Graversen, R. G., and Hazeleger, W.: Arctic winter warming amplified by the thermal inversion and consequent low infrared cooling to space, Nat. Geosci., 4, 758–761, https://doi.org/10.1038/ngeo1285, 2011.

Brooks, I. M., Tjernström, M., Persson, P. O. G., Shupe, M. D., Atkinson, R. A., Canut, G., Birch, C. E., Mauritsen, T., Sedlar, J., and Brooks, B. J.: The Turbulent Structure of the Arctic Summer Boundary Layer During The Arctic Summer Cloud-Ocean Study, Journal of Geophysical Research: Atmospheres, 122, 9685–9704, https://doi.org/10.1002/2017JD027234, 2017.

CLU: Cloud profiling products: Classification, Ice water content, Liquid water content, Categorize; cloud profiling measurements: Lidar; 2019-12-06 to 2020-05-06; from RV Polarstern, Generated by the cloud profiling unit of the ACTRIS Data Centre, https://hdl.handle.net/21.12132/2.b697d787e83344ce, 2023.

Cox, C., Gallagher, M., Shupe, M., Persson, O., Solomon, A., Blomquist, B., Brooks, I., Costa, D., Gottas, D., Hutchings, J., Osborn, J., Morris, S., Preusser, A., and Uttal, T.: 10-meter (m) meteorological flux tower measurements (Level 1 Raw), Multidisciplinary Drifting Observatory for the Study of Arctic Climate (MOSAiC), central Arctic, October 2019 - September 2020, Arctic Data Center, https://doi.org/10.18739/A2VM42Z5F, 2021.

Dai, C., Wang, Q., Kalogiros, J. A., Lenschow, D. H., Gao, Z., and Zhou, M.: Determining Boundary-Layer Height from Aircraft Measurements, Boundary Layer Meteorol., 152, 277–302, https://doi.org/10.1007/s10546-014-9929-z, 2014.

Egerer, U., Gottschalk, M., Siebert, H., Ehrlich, A., and Wendisch, M.: The new BELUGA setup for collocated turbulence and radiation measurements using a tethered balloon: first applications in the cloudy Arctic boundary layer, Atmos. Meas. Tech., 12, 4019–4038, https://doi.org/10.5194/amt-12-4019-2019, 2019.

Esau, I. and Zilitinkevich, S.: On the role of the planetary boundary layer depth in the climate system, in: Adv. Sci. Res., vol. 4, pp. 63–69, Copernicus GmbH, https://doi.org/https://doi.org/10.5194/asr-4-63-2010, 2010.

Frehlich, R., Meillier, Y., Jensen, M. L., and Balsley, B.: Turbulence Measurements with the CIRES Tethered Lifting System during CASES-99: Calibration and Spectral Analysis of Temperature and Velocity, J. Atmos. Sci., 60, 9, 2003.

https://doi.org/10.5194/egusphere-2023-629
Preprint. Discussion started: 13 April 2023

Garratt, J. R.: The atmospheric boundary layer, Cambridge atmospheric and space science series, Cambridge University Press, transferred to digital print. edn., 1997.

Gierens, R., Kneifel, S., Shupe, M. D., Ebell, K., Maturilli, M., and Löhnert, U.: Low-level mixed-phase clouds in a complex Arctic environment, Atmos. Chem. Phys., 20, 3459–3481, https://doi.org/https://doi.org/10.5194/acp-20-3459-2020, 2020.

Grachev, A. A., Andreas, E. L., Fairall, C. W., Guest, P. S., and Persson, P. O. G.: The Critical Richardson Number and Limits of Applicability of Local Similarity Theory in the Stable Boundary Layer, Boundary Layer Meteorol., 147, 51–82, https://doi.org/10.1007/s10546-012-9771-0, 2013.

Graversen, R. G., Mauritsen, T., Tjernström, M., Källén, E., and Svensson, G.: Vertical structure of recent Arctic warming, Nature, 451, 53–56, https://doi.org/10.1038/nature06502, 2008.

Griesche, H. J., Seifert, P., Ansmann, A., Baars, H., Barrientos Velasco, C., Bühl, J., Engelmann, R., Radenz, M., Zhenping, Y., and Macke, A.: Application of the shipborne remote sensing supersite OCEANET for profiling of Arctic aerosols and clouds during *Polarstern* cruise PS106, Atmos. Meas. Tech., 13, 5335–5358, https://doi.org/10.5194/amt-13-5335-2020, 2020.

Griesche, H. J., Ohneiser, K., Seifert, P., Radenz, M., Engelmann, R., and Ansmann, A.: Contrasting ice formation in Arctic clouds: surface-coupled vs. surface-decoupled clouds, Atmos. Chem. Phys., 21, 10 357–10 374, https://doi.org/10.5194/acp-21-10357-2021, 2021.

Heinemann, G. and Rose, L.: Surface energy balance, parameterizations of boundary-layer heights and the application of resistance laws near an Antarctic Ice Shelf front, Boundary Layer Meteorol., 51, 123–158, https://doi.org/10.1007/BF00120464, 1990.

Illingworth, A. J., Hogan, R. J., O'Connor, E. J., Bouniol, D., Brooks, M. E., Delanoé, J., Donovan, D. P., Eastment, J. D., Gaussiat, N., Goddard, J. W. F., Haeffelin, M., Baltink, H. K., Krasnov, O. A., Pelon, J., Piriou, J.-M., Protat, A., Russchenberg, H. W. J., Seifert, A., Tompkins, A. M., Zadelhoff, G.-J. v., Vinit, F., Willén, U., Wilson, D. R., and Wrench, C. L.: Cloudnet: Continuous Evaluation of Cloud Profiles in Seven Operational Models Using Ground-Based Observations, Bull. Amer. Meteor. Soc., 88, 883–898, https://doi.org/10.1175/BAMS-88-6-883, 2007.

Intrieri, J. M., Fairall, C. W., Shupe, M. D., Persson, P. O. G., Andreas, E. L., Guest, P. S., and Moritz, R. E.: An annual cycle of Arctic surface cloud forcing at SHEBA, Journal of Geophysical Research: Oceans, 107, SHE 13–1–SHE 13–14, https://doi.org/10.1029/2000JC000439, 2002a.

Intrieri, J. M., Shupe, M. D., Uttal, T., and McCarty, B. J.: An annual cycle of Arctic cloud characteristics observed by radar and lidar at SHEBA, Journal of Geophysical Research: Oceans, 107, SHE 5–1–SHE 5–15, https://doi.org/10.1029/2000JC000423, 2002b.

Jozef, G., Cassano, J., Dahlke, S., and de Boer, G.: Testing the efficacy of atmospheric boundary layer height detection algorithms using uncrewed aircraft system data from MOSAiC, Atmos. Meas. Tech., 15, 4001–4022, https://doi.org/10.5194/amt-15-4001-2022, 2022.

Kitaigorodskii, S. A.: On the computation of the thickness of the wind-mixing layer in the ocean, Izv. Akad. Nauk Uz SSSR. Ser. Geofiz., 3, 425 – 431, 1960.

Knust, R.: Polar Research and Supply Vessel POLARSTERN Operated by the Alfred-Wegener-Institute, Journal of large-scale research facilities (JLSRF), 3, A119–A119, https://doi.org/10.17815/jlsrf-3-163, 2017.

López-García, V., Neely, III, R. R., Dahlke, S., and Brooks, I. M.: Low-level jets over the Arctic Ocean during MOSAiC, Elementa: Science of the Anthropocene, 10, 00 063, https://doi.org/10.1525/elementa.2022.00063, 2022.

Lüpkes, C., Vihma, T., Jakobson, E., König-Langlo, G., and Tetzlaff, A.: Meteorological observations from ship cruises during summer to the central Arctic: A comparison with reanalysis data, Geophysical Research Letters, 37, https://doi.org/https://doi.org/10.1029/2010GL042724, 2010.

https://doi.org/10.5194/egusphere-2023-629
Preprint. Discussion started: 13 April 2023

Mahrt, L.: Modelling the depth of the stable boundary-layer, Boundary Layer Meteorol., 21, 3–19, https://doi.org/10.1007/BF00119363, 1981.

Maturilli, M., Sommer, M., Holdridge, D. J., Dahlke, S., Graeser, J., Sommerfeld, A., Jaiser, R., Deckelmann, H., and Schulz, A.: MOSAiC radiosonde data (level 3), PANGAEA, https://doi.org/10.1594/PANGAEA.943870, 2022.

Mayfield, J. A. and Fochesatto, G. J.: The Layered Structure of the Winter Atmospheric Boundary Layer in the Interior of Alaska, Journal of Applied Meteorology and Climatology, 52, 953–973, https://doi.org/10.1175/JAMC-D-12-01.1, 2013.

Morrison, H., de Boer, G., Feingold, G., Harrington, J., Shupe, M. D., and Sulia, K.: Resilience of persistent Arctic mixed-phase clouds, Nat. Geosci., 5, 11–17, https://doi.org/10.1038/ngeo1332, 2012.

Nicolaus, M., Perovich, D. K., Spreen, G., Granskog, M. A., von Albedyll, L., Angelopoulos, M., Anhaus, P., Arndt, S., Belter, H. J., Bessonov, V., Birnbaum, G., Brauchle, J., Calmer, R., Cardellach, E., Cheng, B., Clemens-Sewall, D., Dadic, R., Damm, E., de Boer, G., Demir, O., Dethloff, K., Divine, D. V., Fong, A. A., Fons, S., Frey, M. M., Fuchs, N., Gabarró, C., Gerland, S., Goessling, H. F., Gradinger, R., Haapala, J., Haas, C., Hamilton, J., Hannula, H.-R., Hendricks, S., Herber, A., Heuzé, C., Hoppmann, M., Høyland, K. V., Huntemann, M., Hutchings, J. K., Hwang, B., Itkin, P., Jacobi, H.-W., Jaggi, M., Jutila, A., Kaleschke, L., Katlein, C., Kolabutin, N., Krampe, D., Kristensen, S. S., Krumpen, T., Kurtz, N., Lampert, A., Lange, B. A., Lei, R., Light, B., Linhardt, F., Liston, G. E., Loose, B., Macfarlane, A. R., Mahmud, M., Matero, I. O., Maus, S., Morgenstern, A., Naderpour, R., Nandan, V., Niubom, A., Oggier, M., Oppelt, N., Pätzold, F., Perron, C., Petrovsky, T., Pirazzini, R., Polashenski, C., Rabe, B., Raphael, I. A., Regnery, J., Rex, M., Ricker, R., Riemann-Campe, K., Rinke, A., Rohde, J., Salganik, E., Scharien, R. K., Schiller, M., Schneebeli, M., Semmling, M., Shimanchuk, E., Shupe, M. D., Smith, M. M., Smolyanitsky, V., Sokolov, V., Stanton, T., Stroeve, J., Thielke, L., Timofeeva, A., Tonboe, R. T., Tavri, A., Tsamados, M., Wagner, D. N., Watkins, D., Webster, M., and Wendisch, M.: Overview of the MOSAiC expedition: Snow and sea ice, Elementa: Science of the Anthropocene, 10, 000 046, https://doi.org/10.1525/elementa.2021.000046, 2022.

Peng, S., Yang, Q., Shupe, M. D., Xi, X., Han, B., Chen, D., and Liu, C.: Atmospheric boundary layer structure over the Arctic Ocean during MOSAiC, EGUsphere [preprint], pp. 1–31, https://doi.org/10.5194/egusphere-2023-347, publisher: Copernicus GmbH, 2023.

Persson, P. O. G., Fairall, C. W., Andreas, E. L., Guest, P. S., and Perovich, D. K.: Measurements near the Atmospheric Surface Flux Group tower at SHEBA: Near-surface conditions and surface energy budget, Journal of Geophysical Research: Oceans, 107, SHE 21–1–SHE 21–35, https://doi.org/10.1029/2000JC000705, 2002.

Rabe, B., Heuzé, C., Regnery, J., Aksenov, Y., Allerholt, J., Athanase, M., Bai, Y., Basque, C., Bauch, D., Baumann, T. M., Chen, D., Cole, S. T., Craw, L., Davies, A., Damm, E., Dethloff, K., Divine, D. V., Doglioni, F., Ebert, F., Fang, Y.-C., Fer, I., Fong, A. A., Gradinger, R., Granskog, M. A., Graupner, R., Haas, C., He, H., He, Y., Hoppmann, M., Janout, M., Kadko, D., Kanzow, T., Karam, S., Kawaguchi, Y., Koenig, Z., Kong, B., Krishfield, R. A., Krumpen, T., Kuhlmey, D., Kuznetsov, I., Lan, M., Laukert, G., Lei, R., Li, T., Torres-Valdés, S., Lin, L., Lin, L., Liu, H., Liu, N., Loose, B., Ma, X., McKay, R., Mallet, M., Mallett, R. D. C., Maslowski, W., Mertens, C., Mohrholz, V., Muilwijk, M., Nicolaus, M., O'Brien, J. K., Perovich, D., Ren, J., Rex, M., Ribeiro, N., Rinke, A., Schaffer, J., Schuffenhauer, I., Schulz, K., Shupe, M. D., Shaw, W., Sokolov, V., Sommerfeld, A., Spreen, G., Stanton, T., Stephens, M., Su, J., Sukhikh, N., Sundfjord, A., Thomisch, K., Tippenhauer, S., Toole, J. M., Vredenborg, M., Walter, M., Wang, H., Wang, L., Wang, Y., Wendisch, M., Zhao, J., Zhou, M., and Zhu, J.: Overview of the MOSAiC expedition: Physical oceanography, Elementa: Science of the Anthropocene, 10, 00 062, https://doi.org/10.1525/elementa.2021.00062, 2022.

Sedlar, J. and Tjernström, M.: Stratiform Cloud—Inversion Characterization During the Arctic Melt Season, Boundary Layer Meteorol., 132, 455–474, https://doi.org/10.1007/s10546-009-9407-1, 2009.

https://doi.org/10.5194/egusphere-2023-629
Preprint. Discussion started: 13 April 2023

Serreze, M. C. and Barry, R. G.: Processes and impacts of Arctic amplification: A research synthesis, Global and Planetary Change, 77, 85–96, https://doi.org/10.1016/j.gloplacha.2011.03.004, 2011.

Shupe, M. D. and Intrieri, J. M.: Cloud Radiative Forcing of the Arctic Surface: The Influence of Cloud Properties, Surface Albedo, and Solar Zenith Angle, Journal of Climate, 17, 616–628, https://doi.org/10.1175/1520-0442(2004)017<0616:CRFOTA>2.0.CO;2, 2004.

Shupe, M. D., Persson, P. O. G., Brooks, I. M., Tjernström, M., Sedlar, J., Mauritsen, T., Sjogren, S., and Leck, C.: Cloud and boundary layer interactions over the Arctic sea ice in late summer, Atmos. Chem. Phys., 13, 9379–9399, https://doi.org/https://doi.org/10.5194/acp-13-9379-2013, 2013.

Shupe, M. D., Rex, M., Blomquist, B., Persson, P. O. G., Schmale, J., Uttal, T., Althausen, D., Angot, H., Archer, S., Bariteau, L., Beck, I., Bilberry, J., Bucci, S., Buck, C., Boyer, M., Brasseur, Z., Brooks, I. M., Calmer, R., Cassano, J., Castro, V., Chu, D., Costa, D., Cox, C. J., Creamean, J., Crewell, S., Dahlke, S., Damm, E., de Boer, G., Deckelmann, H., Dethloff, K., Dütsch, M., Ebell, K., Ehrlich, A., Ellis, J., Engelmann, R., Fong, A. A., Frey, M. M., Gallagher, M. R., Ganzeveld, L., Gradinger, R., Graeser, J., Greenamyer, V., Griesche, H., Griffiths, S., Hamilton, J., Heinemann, G., Helmig, D., Herber, A., Heuzé, C., Hofer, J., Houchens, T., Howard, D., Inoue, J., Jacobi, H.-W., Jaiser, R., Jokinen, T., Jourdan, O., Jozef, G., King, W., Kirchgaessner, A., Klingebiel, M., Krassovski, M., Krumpen, T., Lampert, A., Landing, W., Laurila, T., Lawrence, D., Lonardi, M., Loose, B., Lüpkes, C., Maahn, M., Macke, A., Maslowski, W., Marsay, C., Maturilli, M., Mech, M., Morris, S., Moser, M., Nicolaus, M., Ortega, P., Osborn, J., Pätzold, F., Perovich, D. K., Petäjä, T., Pilz, C., Pirazzini, R., Posman, K., Powers, H., Pratt, K. A., Preußer, A., Quéléver, L., Radenz, M., Rabe, B., Rinke, A., Sachs, T., Schulz, A., Siebert, H., Silva, T., Solomon, A., Sommerfeld, A., Spreen, G., Stephens, M., Stohl, A., Svensson, G., Uin, J., Viegas, J., Voigt, C., von der Gathen, P., Wehner, B., Welker, J. M., Wendisch, M., Werner, M., Xie, Z., and Yue, F.: Overview of the MOSAiC expedition: Atmosphere, Elementa: Science of the Anthropocene, 10, 00 060, https://doi.org/10.1525/elementa.2021.00060, 2022.

Siebert, H., Lehmann, K., and Wendisch, M.: Observations of Small-Scale Turbulence and Energy Dissipation Rates in the Cloudy Boundary Layer, J. Atmos. Sci., 63, 1451–1466, https://doi.org/10.1175/JAS3687.1, 2006.

Stramler, K., Genio, A. D. D., and Rossow, W. B.: Synoptically Driven Arctic Winter States, Journal of Climate, 24, 1747–1762, https://doi.org/10.1175/2010JCLI3817.1, 2011.

Stull, R. B.: An introduction to boundary layer meteorology., Kluwer Academic Publishers, Dordrecht, The Netherlands, 666 p., 1988.

Tjernström, M. and Graversen, R. G.: The vertical structure of the lower Arctic troposphere analysed from observations and the ERA-40 reanalysis, Quart. J. Roy. Meteor. Soc., 135, 431–443, https://doi.org/10.1002/qj.380, 2009.

Turner, D. D., Shupe, M. D., and Zwink, A. B.: Characteristic Atmospheric Radiative Heating Rate Profiles in Arctic Clouds as Observed at Barrow, Alaska, Journal of Applied Meteorology and Climatology, 57, 953–968, https://doi.org/10.1175/JAMC-D-17-0252.1, 2018.

Vickers, D. and Mahrt, L.: Evaluating Formulations of Stable Boundary Layer Height, Journal of Applied Meteorology, 43, 1736–1749, https://doi.org/10.1175/JAM2160.1, 2004.

Wendisch, M., Macke, A., Ehrlich, A., Lüpkes, C., Mech, M., Chechin, D., Dethloff, K., Velasco, C. B., Brückner, M., Clemen, H.-C., Crewell, S., Donth, T., Dupuy, R., Egerer, U., Engelmann, R., Engler, C., Eppers, O., Gehrmann, M., Gong, X., Gourbeyre, C., Griesche, H., Hartmann, J., Hartmann, M., Heinold, B., Herber, A., Herrmann, H., Heygster, G., Hoor, P., Jafariserajehlou, S., Jäkel, E., Jourdan, O., Kästner, U., Kecorius, S., Knudsen, E. M., Köllner, F., Kretzschmar, J., Lelli, L., Leroy, D., Maturilli, M., Mei, L., Mertes, S., Mioche, G., Neuber, R., Nicolaus, M., Nomokonova, T., Notholt, J., Palm, M., van Pinxteren, M., Quaas, J., Richter, P., Ruiz-Donoso, E., Schäfer, M., Schmieder, K., Schnaiter, M., Schneider, J., Schwarzenböck, A., Seifert, P., Shupe, M. D., Siebert, H., Spreen, G., Stapf, J., Vogl, T., Welti, A., Wex, H., Zanatta, M., and Zeppenfeld, S.: The Arctic Cloud Puzzle: Using ACLOUD/PASCAL Multiplatform Observations to Unravel the Role of Clouds and Aerosol Particles in Arctic Amplification, Bull. Amer. Meteor. Soc., 5, 841 – 871, 2019.

https://doi.org/10.5194/egusphere-2023-629
Preprint. Discussion started: 13 April 2023

Wendisch, M., Brückner, M., Crewell, S., Ehrlich, A., Notholt, J., Lüpkes, C., Macke, A., Burrows, J. P., Rinke, A., Quaas, J., Maturilli, M., Schemann, V., Shupe, M. D., Akansu, E. F., Barrientos-Velasco, C., Bärfuss, K., Blechschmidt, A.-M., Block, K., Bougoudis, I., Bozem, H., Böckmann, C., Bracher, A., Bresson, H., Bretschneider, L., Buschmann, M., Chechin, D. G., Chylik, J., Dahlke, S., Deneke, H., Dethloff, K., Donth, T., Dorn, W., Dupuy, R., Ebell, K., Egerer, U., Engelmann, R., Eppers, O., Gerdes, R., Gierens, R., Gorodetskaya, I. V., Gottschalk, M., Griesche, H., Gryanik, V. M., Handorf, D., Harm-Altstädter, B., Hartmann, J., Hartmann, M., Heinold, B., Herber, A., Herrmann, H., Heygster, G., Höschel, I., Hofmann, Z., Hölemann, J., Hünerbein, A., Jafariserajehlou, S., Jäkel, E., Jacobi, C., Janout, M., Jansen, F., Jourdan, O., Jurányi, Z., Kalesse-Los, H., Kanzow, T., Käthner, R., Kliesch, L. L., Klingebiel, M., Knudsen, E. M., Kovács, T., Körtke, W., Krampe, D., Kretzschmar, J., Kreyling, D., Kulla, B., Kunkel, D., Lampert, A., Lauer, M., Lelli, L., Lerber, A. v., Linke, O., Löhnert, U., Lonardi, M., Losa, S. N., Losch, M., Maahn, M., Mech, M., Mei, L., Mertes, S., Metzner, E., Mewes, D., Michaelis, J., Mioche, G., Moser, M., Nakoudi, K., Neggers, R., Neuber, R., Nomokonova, T., Oelker, J., Papakonstantinou-Presvelou, I., Pätzold, F., Pefanis, V., Pohl, C., Pinxteren, M. v., Radovan, A., Rhein, M., Rex, M., Richter, A., Risse, N., Ritter, C., Rostosky, P., Rozanov, V. V., Donoso, E. R., Garfias, P. S., Salzmann, M., Schacht, J., Schäfer, M., Schneider, J., Schnierstein, N., Seifert, P., Seo, S., Siebert, H., Soppa, M. A., Spreen, G., Stachlewska, I. S., Stapf, J., Stratmann, F., Tegen, I., Viceto, C., Voigt, C., Vountas, M., Walbröl, A., Walter, M., Wehner, B., Wex, H., Willmes, S., Zanatta, M., and Zeppenfeld, S.: Atmospheric and Surface Processes, and Feedback Mechanisms Determining Arctic Amplification: A Review of First Results and Prospects of the (AC)3 Project, Bull. Amer. Meteor. Soc., 104, E208–E242, https://doi.org/10.1175/BAMS-D-21-0218.1, 2023.

Wyngaard, J. C.: Turbulence in the atmosphere, Cambridge University Press, 1. publ., repr. edn., 2012.

Zhang, Y., Gao, Z., Li, D., Li, Y., Zhang, N., Zhao, X., and Chen, J.: On the computation of planetary boundary-layer height using the bulk Richardson number method, Geosci. Model Dev., 7, 2599–2611, https://doi.org/10.5194/gmd-7-2599-2014, 2014.

Zilitinkevich, S.: On the determination of the height of the Ekman boundary layer., Boundary Layer Meteorol., 3, 141 – 145, 1972.

Zilitinkevich, S. and Baklanov, A.: Calculation Of The Height Of The Stable Boundary Layer In Practical Applications, Boundary Layer Meteorol., 105, 389–409, https://doi.org/10.1023/A:1020376832738, 2002.